frontiers in Earth Science

ORIGINAL RESEARCH
published: 28 March 2022
doi: 10.3389/feart.2022.849438

Numerical Modeling of an Umbrella-Shaped Bolt and Its Anchorage Characteristics in Rock Engineering

Yong Xiong[1], *Hang Chen*[1], *Yonghui Cheng*[1]*, *Shenggang Hu*[1], *Zhaofeng Wang*[2,3] and *Yaohui Gao*[4]

[1]Key Laboratory of Geotechnical Mechanics and Engineering of Ministry of Water Resources, Changjiang River Scientific Reseatch Institute, Wuhan, China, [2]Institute of Rock and Soil Mechanics, Chinese Academy of Sciences, Wuhan, China, [3]State Key Laboratory of Geomechanics and Geotechnical Engineering, University of Chinese Academy of Sciences, Beijing, China, [4]Hydropower Engineering Institute, Power China Huadong Engineering Corporation Limited, Hangzhou, China

The umbrella-shaped bolt (U-bolt) is a novel type of mechanical bolt used for rock reinforcement. It is made of a smooth steel bar, hinges, rigid rods, and sliding blocks. During installation and operation, the tension of the bolt is converted into the extrusion force on the rock mass deep in slope, so that the higher compressive strength of the rock mass is used to obtain the greater friction force and anchoring force. In this article, the structural and mechanical analysis results of the U-bolt is provided, and the relation between penetration and point normal stress is discussed. Based on these analyses, a simulation method for the U-bolt is proposed. The bolt elements are identified at first, then the penetration on the rock mass is calculated, and the tensile strength of bolt elements is increased to a reasonable value. Meanwhile, the method is applied to deep-buried rock reinforcement and a rock slope, and simulation results reveal that the U-bolt can alleviate the fracturing degree and reduce the depth and displacement of the excavation damaged zone (EDZ), and decrease the landslide distance.

Keywords: umbrella-shaped bolt, structural analysis, simulation method, excavation damaged zone, rock supporting

OPEN ACCESS

Edited by:
Yun Zheng,
Institute of Rock and Soil Mechanics (CAS), China

Reviewed by:
Xianjie Hao,
China University of Mining and Technology, China
Rui Rui,
Wuhan University of Technology, China

***Correspondence:**
Yonghui Cheng
chengyh@mail.crsri.cn

Specialty section:
This article was submitted to Geohazards and Georisks, a section of the journal Frontiers in Earth Science

Received: *06 January 2022*
Accepted: *18 February 2022*
Published: *28 March 2022*

Citation:
Xiong Y, Chen H, Cheng Y, Hu S, Wang Z and Gao Y (2022) Numerical Modeling of an Umbrella-Shaped Bolt and Its Anchorage Characteristics in Rock Engineering. Front. Earth Sci. 10:849438. doi: 10.3389/feart.2022.849438

1 INTRODUCTION

The sustainability of underground caves (such as tunnels and caves) is mainly determined by three factors: rock quality, *in situ* stress, and the size or geometry of the cave (Li, 2012). The stress of shallow rock engineering is usually low, and the main stability problem is that the rock falls under gravity (Bizjak and Petkovšek, 2004). In the case of deep-buried hard rock engineering, the rock mass is usually hard and brittle, and the tensile failure should be the main mechanism (Su et al., 2017). In general, the loosened rock blocks or fractured rock mass can be stabilized by installing internal support devices like rock bolts (Cai et al., 2004). Therefore, the bearing capacity of the bolt is a crucial parameter in rock engineering (Chen, 2014).

Meanwhile, a rock slope is also a common kind of rock engineering. Its failure mechanisms and stability have been continuously investigated by researchers in ways of numerical methods, limit equilibrium methods (Aydan and Kawamoto, 1992; Zheng et al., 2018), and other new methods (Zheng et al., 2021). Swelling prestressed bolts and its use in the mechanized excavation of large-section tunnels (Liu et al., 2018), and also prestressed hollow grouting anchor rock burst

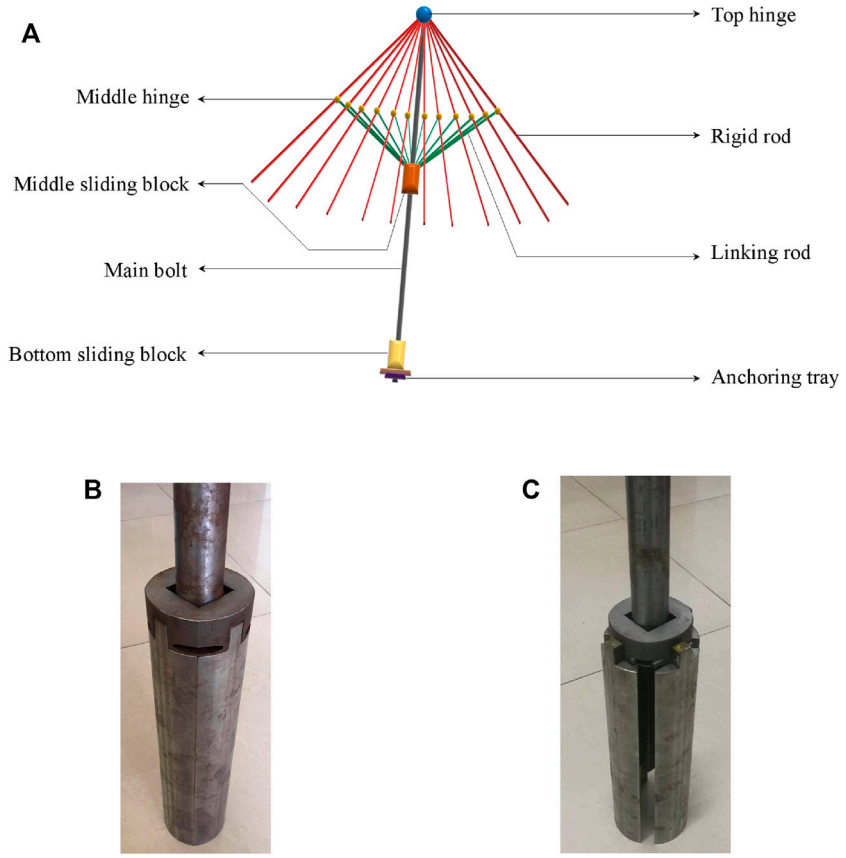

FIGURE 1 | Umbrella-shaped bolt, in which **(A)** the sketch figure, **(B)** bolt image in packing state, and **(C)** bolt image in opening state.

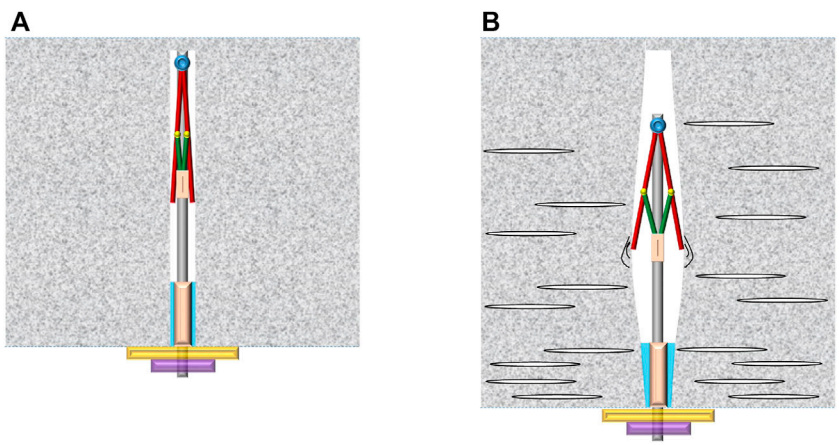

FIGURE 2 | Installation and operation of the U-bolt, in which **(A)** installation and **(B)** operation.

prevention tunnel design (Wang and He, 2011). To strengthen the stability of rock slopes, using rock bolts is a common measure, such as grouting bolt, mechanical shell-expanding bolt, and other new types of bolts. These rock bolts mentioned before have solved engineering problems faced in the process of tunnel construction.

Numerous studies have been carried out on rock bolts, and various types of bolts with high load capacity and high

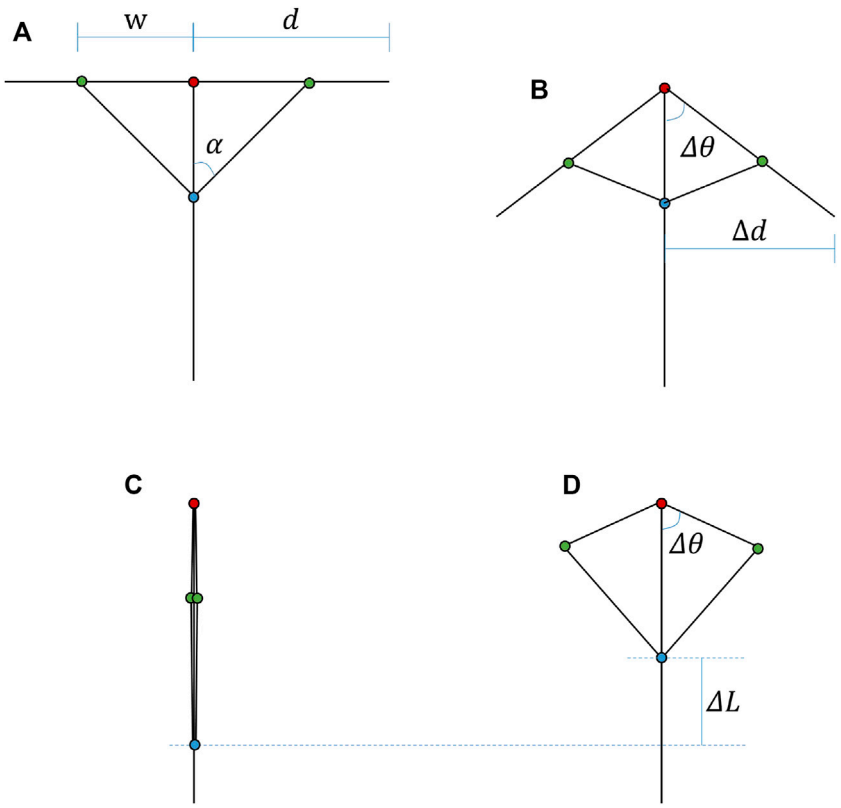

FIGURE 3 | Geometry structure of the U-bolt, where **(A)** the structure when U-bolt is totally expanding, **(B)** the structure when U-bolt is working, **(C)** the structure when U-bolt is installing, and **(D)** geometry shape of main bolt, rigid rod, and linking rod.

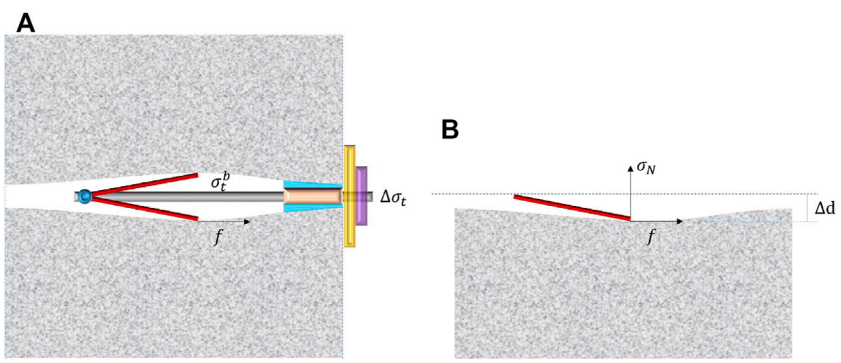

FIGURE 4 | Force analysis of the U-bolt, where **(A)** all forces and **(B)** the force on the internal surface of bore hole.

deformation capacity have been successfully developed and applied, such as cone bolts, Garford bolts, and D-bolts. The cone bolt is the first energy-absorbing-type bolts, and its rejuvenated anchor consists of a smooth steel rod with a flat, running flame forged at the distal end (Li et al., 2014), which can withstand significant deformation of the rock mass by allowing the rejuvenated anchor to move in the grouting materials such as the mortar and the resin. The Garford bolt developed in Australia consists of smooth reinforcement, unique technical anchor, and steel hull at the distal end of the anchor (Varden et al., 2008; Li et al., 2014), in which the inner diameter of the anchor is smaller than that of the bar inside the sleeve. After the rock is deformed, the bolt starts extruding from the inner hole of the bolt, absorbing the enormous energy generated by the expansion of the rock. The D-bolt developed in Norway consists of a smooth steel rod and several bolts used in the deep construction to prevent the tunnel from collapsing because of the rock

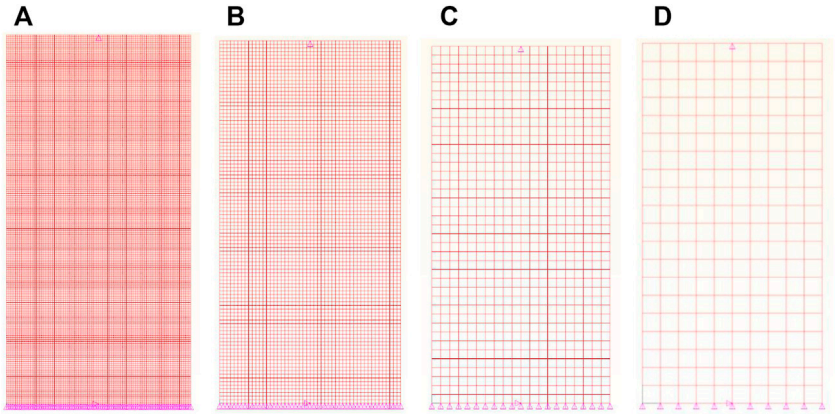

FIGURE 5 | Four grids to study the relation between penetration and point normal stress, in which the element size is set as **(A)** 0.5 mm, **(B)** 1 mm, **(C)** 2.5 mm, and **(D)** 5 mm.

TABLE 1 | Mechanical parameter settings of simulating point loading tests.

No.	Elastic modulus (GPa)	Poisson's ratio	No.	Elastic modulus (GPa)	Poisson's ratio	No.	Elastic modulus (GPa)	Poisson's ratio	No.	Elastic modulus (GPa)	Poisson's ratio
1	1	0.05	13	2	0.2	25	3	0.35	37	5	0.05
2	1	0.1	14	2	0.25	26	3	0.4	38	5	0.1
3	1	0.15	15	2	0.3	27	3	0.45	39	5	0.15
4	1	0.2	16	2	0.35	28	4	0.05	40	5	0.2
5	1	0.25	17	2	0.4	29	4	0.1	41	5	0.25
6	1	0.3	18	2	0.45	30	4	0.15	42	5	0.3
7	1	0.35	19	3	0.05	31	4	0.2	43	5	0.35
8	1	0.4	20	3	0.1	32	4	0.25	44	5	0.4
9	1	0.45	21	3	0.15	33	4	0.3	45	5	0.45
10	2	0.05	22	3	0.2	34	4	0.35			
11	2	0.1	23	3	0.25	35	4	0.4			
12	2	0.15	24	3	0.3	36	4	0.45			

burst. The D-bolt can achieve both high loading capacity and deformability by the elongation of the steel bar between anchors (Li, 2010; Li et al., 2014). These energy-absorbing bolts are considered as important support materials for rock breaking and for the crushing of soil treasures in underground construction. Generally speaking, these energy-absorbing rock bolts are considered as important support materials for rock fracturing and fragmentation.

In this study, a novel umbrella-shaped bolt (U-bolt) was proposed. It is mainly composed of hinges and rigid rods and uses the compression and friction to obtain the anchoring force. The new bolt is introduced in **Section 2**, concentrating on the structural and mechanical analyses of U-bolts, and the relation between penetration and point normal stress was discussed. The numerical model establishment method for U-bolts was described in **Section 3**. This method was then applied to the U-bolt simulation of the rock tunnel excavation and rock slope in **Section 4**, and the performance of U-bolts was compared between no supporting and U-bolt-supporting cases.

TABLE 2 | Fitting coefficients and R square of the relation between the normal stiffness K against the elastic modulus E and Poisson's ratio v.

Element size (mm)	a	b	R Square (%)
0.5	382.2	0.3797	99.99
1	209.4	0.3773	99.98
2.5	95.89	0.3697	99.99
5	53.85	0.3685	99.99

2 STRUCTURAL ANALYSIS

2.1 Basic Description of Umbrella-Shaped Bolt

As shown in **Figure 1A**, the umbrella-shaped bolt consists of the top hinge, the rigid rod, the linking rod, the anchoring tray, the bottom sliding block, the main bolt, the middle sliding block, and the middle hinge. Many rigid rods are connected to the main bolt through the top hinge, and they are also connected with the corresponding linking rods with the middle hinge. The linking rod can move with the middle sliding block along the main bolt.

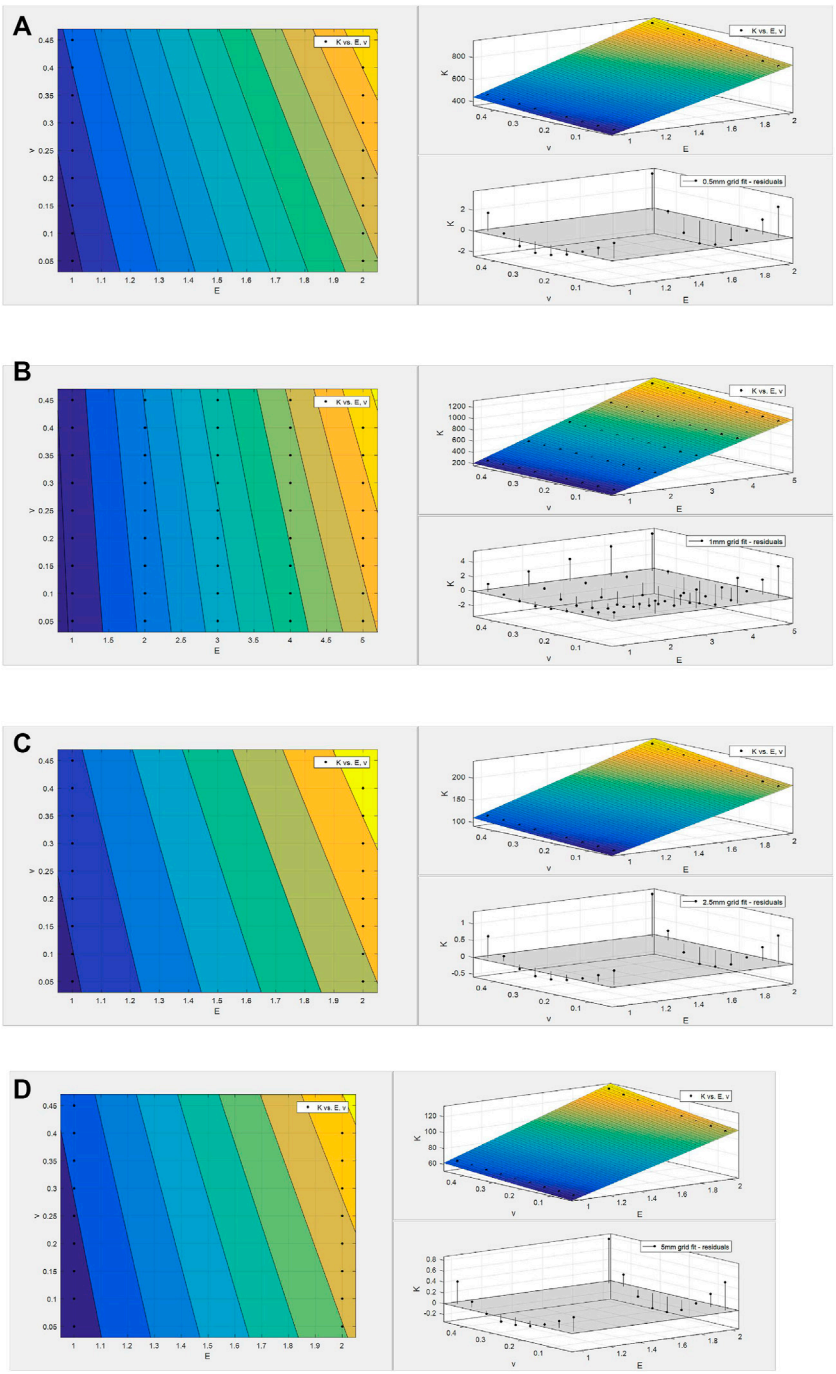

FIGURE 6 | Fitting results of stiffness K against the elastic modulus E and Poisson's ratio v, in which the element size is **(A)** 0.5 mm, **(B)** 1 mm, **(C)** 2.5 mm, and **(D)** 5 mm.

In addition, there is also a bottom sliding block adhering to the anchoring tray. The bolt in the packing state (**Figure 1B**) and opening state (**Figure 1C**) is also illustrated.

During installation (as illustrated in **Figure 2A**), a bore hole with a reasonable dimension is drilled at first and the U-bolt is then inserted into the hole of the rock mass. Both the rigid rods and linking rods shrink together, which are close to the main bolt in this process. The bottom sliding block is adhered to the rock mass with glue, and the anchoring tray is fixed on the surface of the internal tunnel free face.

When the rock mass initiates dilation with many excavation-induced fractures (as shown in **Figure 2B**), the whole section begins to expand (Wang et al., 2020). The main bolt then starts to extend, and the rigid rods initiate expanding. They squeeze the internal face

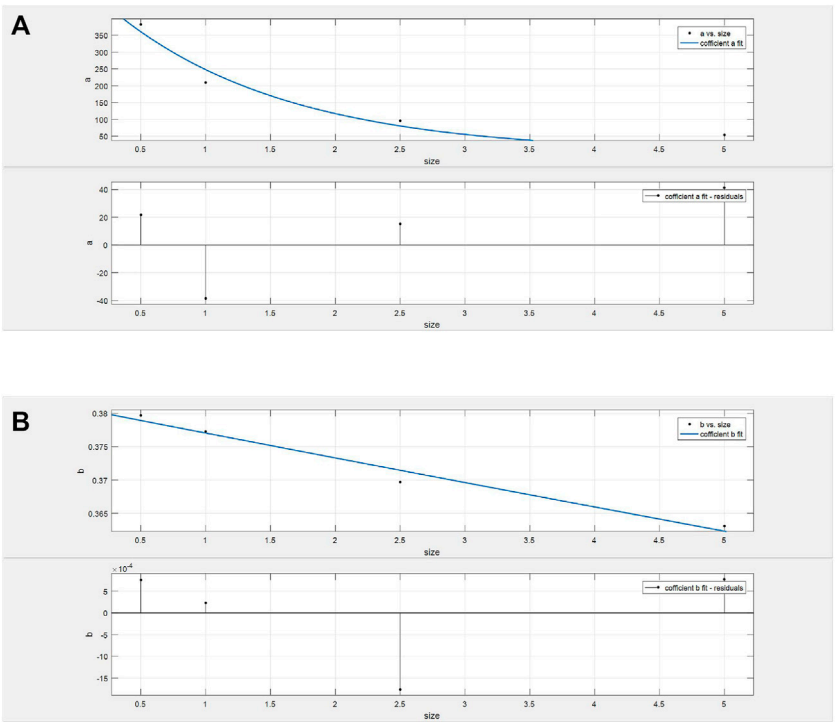

FIGURE 7 | Fitting results of coefficients against element sizes, where **(A)** coefficient *a* and **(B)** coefficient *b*.

of the bore hole, and friction emerges between the internal face and the rigid rod. This friction and the tensile strength inhibit the dilation of the rock mass. Generally speaking, the tension of the bolt is converted into the extrusion force on the rock mass, and the higher the compressive strength of the rock mass is, the greater the friction force and anchoring force the bolt can obtain.

2.2 Force Analysis

The mechanical analysis is studied in this section. As shown in **Figure 3A**, when the U-bolt is totally expanding, we define the distance between the top and middle hinges as width w, and the distance between the top hinge and the end of the rigid rod as distance d. The angle between the main bolt and the linking rod is α, and the length of the linking rod can be calculated as follows:

$$l = \frac{w}{sin\alpha}. \tag{1}$$

As illustrated in **Figure 3B**, when the U-bolt is working, the opening angle is defined as Δθ, and the expanding length can be acquired as follows:

$$\Delta d = d \cdot sin\Delta\theta. \tag{2}$$

In **Figure 3C**, we can find that the initial position distance between the top hinge and middle sliding block can be obtained as follows:

$$D = l + w. \tag{3}$$

The law of cosines (Lee, 1997) will be satisfied (as shown in **Figure 3D**), and the relation between the opening angle Δθ and the extension length ΔL is shown as follows:

$$\cos\Delta\theta = \frac{(D-\Delta L)^2 + d^2 - l^2}{2d(D-\Delta L)}. \tag{4}$$

Combining **Eqs 1**–**4**, we get

$$\Delta d = d \cdot \sqrt{1 - \frac{(D-\Delta L)^2 + d^2 - l^2}{2d(D-\Delta L)}}. \tag{5}$$

In the reasonable range of ΔL, the expanding length Δd monotonically increases with the extension length ΔL.

When the U-bolt is working (**Figure 4A**), the additional tensile stress is provided with two parts, including the tensile strength σ_t^b of the main bolt and the friction f between the bore hole inner face and the rigid rod, which indicates that

$$\Delta\sigma_t = \sigma_t^b + f. \tag{6}$$

As illustrated in **Figure 4B**, the friction can be calculated according to the Coulomb criterion (Renard, 2006), which means that

$$f = \mu\sigma_N, \tag{7}$$

where μ is the friction coefficient and σ_N is the normal stress.

The expanding length Δd in **Figures 3B**, **4B** is also known as the penetration; therefore, the normal force σ_N can be defined by a linear relation (1) as follows:

$$\sigma_N = K\Delta d, \tag{8}$$

where K is the contact stiffness, and relation between penetration and the point normal stress will be discussed in the next section.

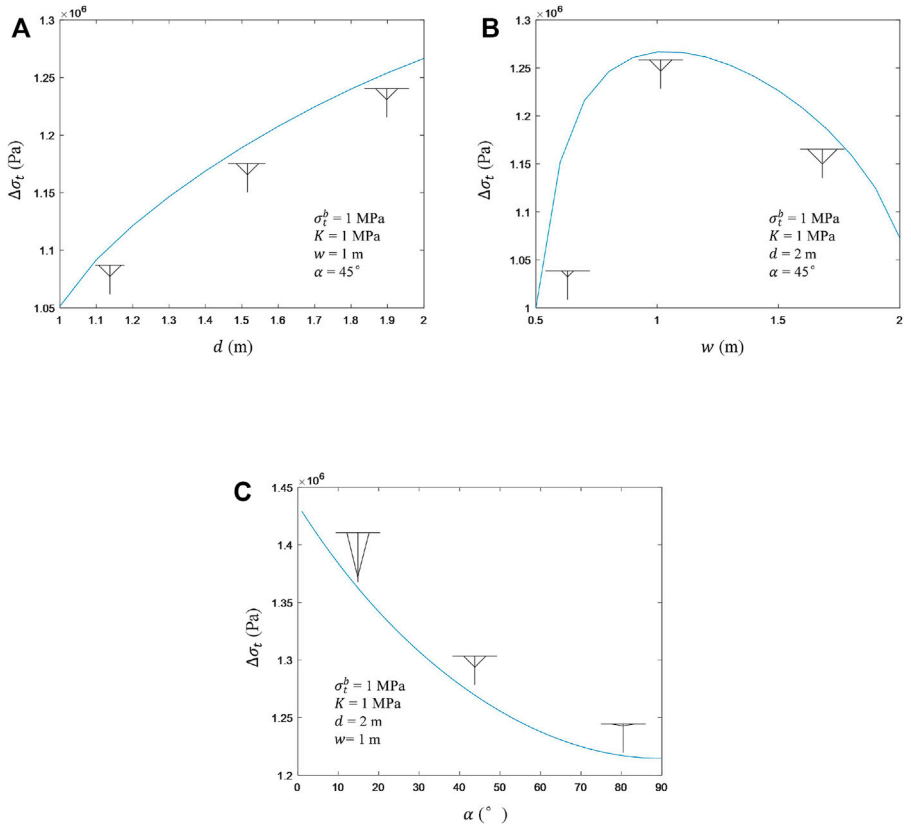

FIGURE 8 | Sensibility analysis of the structural parameters d, w, and α. **(A), (B)**, and **(C)** are the influences of d, w, and α to the enhanced tensile strength, respectively.

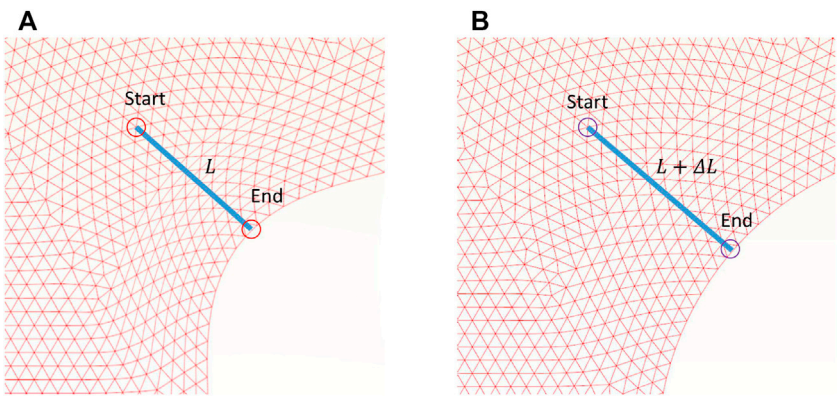

FIGURE 9 | Calculation of the penetration, in which **(A)** the moment when U-bolt installs, and **(B)** the moment when U-bolt is working.

2.3 Relation Between Penetration and Point Normal Stress

As pointed out in **Eq. 8**, in order to study the relation between the penetration and the point normal stress, it is better to establish the relation between the stiffness and the penetration in **Eq. 8**. Here, a numerical approach is provided, and the analysis zone is considered as an elastic body.

As illustrated in **Figure 5**, four simulation grids are set, including 0.5 mm (**Figure 5A**), 1 mm (**Figure 5B**), 2.5 mm (**Figure 5C**), and 5 mm (**Figure 5D**). The size of all these four grids is 0.5 mm × 0.1 mm, and the aspect ratios are all 2 to eliminate the influence of the aspect ratio effect. The bottom edge of these simulation specimens is fixed at the vertical direction, and the middle of the bottom edge is also fixed at the horizontal

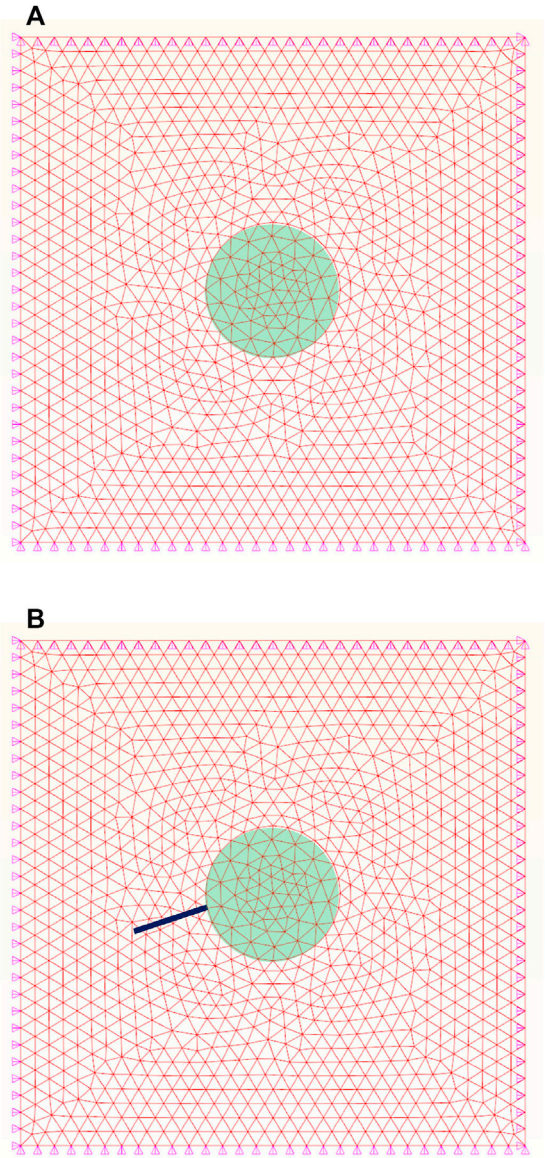

FIGURE 10 | Simulation setup, where **(A)** no support and **(B)** support with U-bolt.

direction. Only the middle of the top edge is vertical displacement loading representing the point loading.

At least 18 simulation tests were conducted for each grid, and the mechanical properties are listed in **Table 1**. It should be noted that 45 tests were conducted for 0.05 mm element size, and 18 tests (Nos. 1~18 in **Table 1**) were conducted for other element sizes.

A fitting function between the normal stiffness K_n against the elastic modulus E and Poisson's ratio v is established as follows:

$$K_n = \frac{aE}{1 - bv}, \tag{9}$$

where a and b are the fitting coefficients. The fitting coefficients and R square are provided in **Table 2**. As the simulation is conduction for the elastic body, the R squares for all the element sizes are close to 1, and the fitting function (**Figures 6A–D**) performs well.

The element size effect is also considered, an exponent function is proposed, and the following relation is obtained:

$$a = 524.3e^{-0.7489s}, \tag{10.1}$$

$$b = 0.3808e^{-0.0099s}, \tag{10.2}$$

where s is the element size. The fitting results are illustrated in **Figures 7A,B**. The R square for the coefficient a is 93.96%, and that for b is 97.46%, and they all have relatively good fitting performances.

Combing all these equations, the enhanced tensile strength provided by the U-bolt can be calculated as follows:

$$\Delta\sigma_t = \sigma_t^b + \mu\frac{524.3e^{-0.7489s}E}{1 - 0.3808e^{-0.0099s}v}d \cdot \sqrt{1 - \frac{\left(w + \frac{w}{\sin\alpha} - \Delta L\right)^2 + d^2 - \left(\frac{w}{\sin\alpha}\right)^2}{2d\left(w + \frac{w}{\sin\alpha} - \Delta L\right)}}. \tag{11}$$

In **Eq. 11**, there are only 8 parameters that need to be determined, of which E, v, and μ are the mechanical properties of the rock mass, which is known before simulation. σ_t^b is the tensile strength of the main bolt; d, w, and α are the structural parameters of the U-bolt, and they determine the reinforcement ability of the U-bolt. Only s and ΔL are the variables which need to be determined during the simulation. For the structural parameters d, w, and α, the sensibility analysis has been conducted, as illustrated in **Figure 5**, in order to study the influence of them. The results indicate that the enhanced tensile strength increases with the increase in d and decreases with the increase in α. With the increase in w, the enhanced tensile strength increases at first and then decreases.

3 NUMERICAL IMPLEMENTATION

3.1 Basic Framework

The numerical implementation of the U-bolt follows a simple framework, which is finding the element where bolts go through (they are defined as the bolt elements), then calculating the enhanced tensile strength based on the extension length ΔL, and finally adding the enhanced tensile strength to the current strength of the bolt elements. These processes will be introduced in detail in the next sections.

TABLE 3 | Crustal stress of the simulated tunnel.

σ_x (MPa)	σ_y (MPa)	τ_{xy} (MPa)
10	30	5

TABLE 4 | Mechanical properties of the simulated tunnel.

	Origin rock mass	Fractured rock mass	Failed rock mass (residual)
Elastic modulus (GPa)	10	10	10
Poisson's ratio	0.3	0.3	0.3
Cohesion strength (MPa)	10	1	1
Friction angle (°)	20	20	40
Tensile strength (MPa)	5	1	1
Critical plastic strain (‰)	0	2	4

TABLE 5 | U-bolt parameters.

Tensile strength (MPa)	d (m)	w (m)	α (°)
10	2	1	45

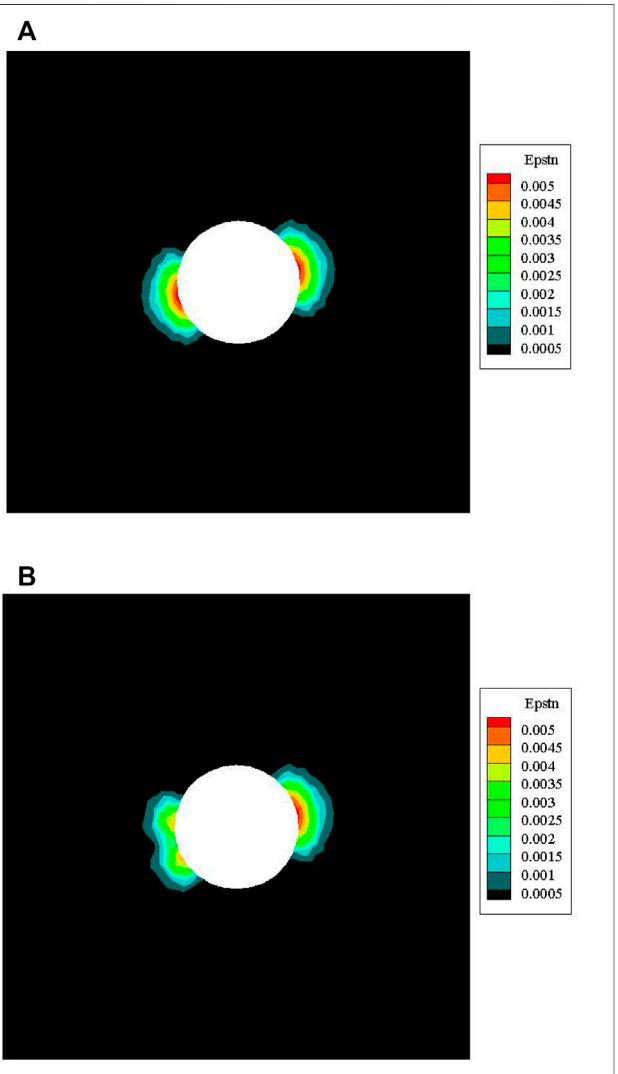

FIGURE 11 | Simulated equivalent plastic strain results, in which **(A)** no support and **(B)** support with U-bolt.

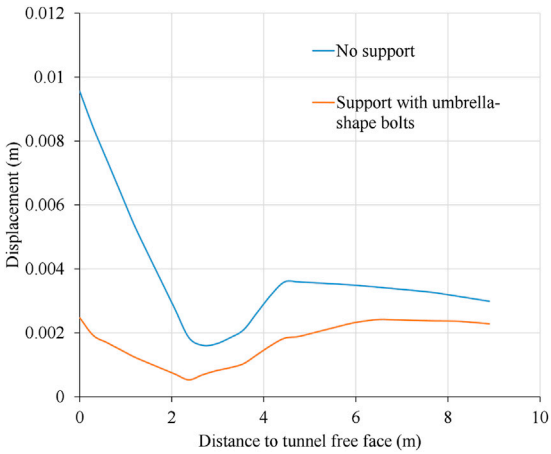

FIGURE 12 | Comparison of the displacement evolution results along the bolt direction for no support and support with U-bolt cases. In addition, the result is the displacement plotted against the distance to tunnel-free face.

3.2 Identification of Bolt Elements

The bolt elements are identified at the beginning of the simulation. There are three cases that emerge during the identification of bolt elements, as shown in **Figure 8**, including case A where the bolt does not go through any node of the bolt element, case B where the bolt goes through 1 node of the bolt element, and case C where the bolt goes through 2 nodes of the bolt element.

For cases A and B, it is easy to point out the bolt element through elements where the bolt cut across. For case C, it may be a little different, in which the 2 elements with opposite positions where the bolt goes through are all treated as the bolt elements.

3.3 Calculation of the Penetration

Figure 9 shows two moments of the U-bolt operation in the simulation. For **Figure 9A**, when the bolt is installed, the initial length of the U-bolt will be calculated using the following equation:

$$L = \left|\left[\left(x^{start} + u_x^{start}\right) - \left(x^{end} + u_x^{end}\right)\right]cos\beta + \left[\left(y^{start} + u_y^{start}\right) - \left(y^{end} + u_y^{end}\right)\right]sin\beta\right|, \quad (12)$$

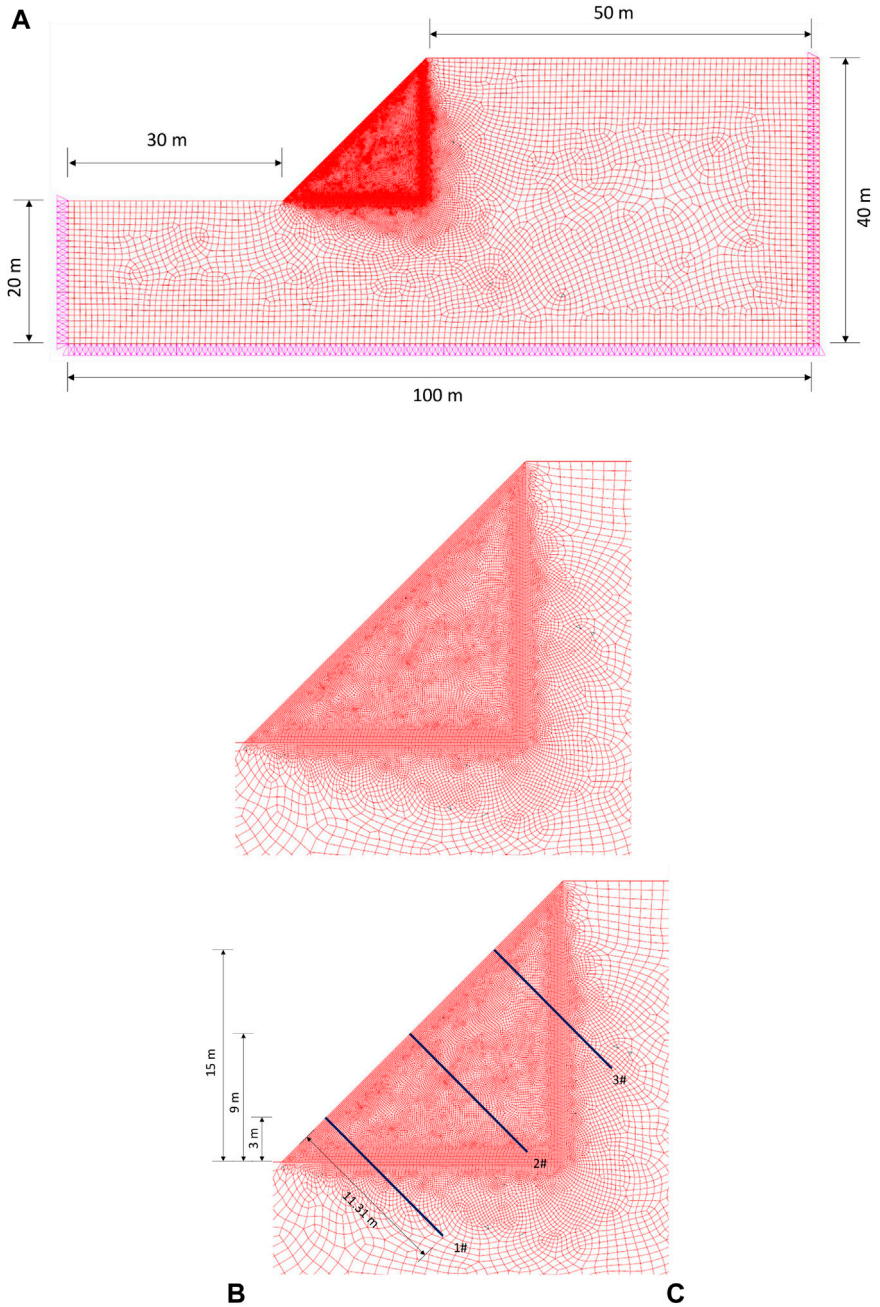

FIGURE 13 | Simulation setup of the rock slope, where **(A)** the simulation mesh and boundary set, **(B)** no support model, and **(C)** support model with U-bolt.

where x^{start}, y^{start}, x^{end}, and y^{end} are the horizontal and vertical positions of the two ends of the U-bolt, and u_x^{start}, u_y^{start}, u_x^{end}, and u_y^{end} are the horizontal and vertical displacements of the two ends of the U-bolt. β is the installation angle which is the angle between the U-bolt and the horizontal line, and it can be obtained as follows:

$$\beta = \operatorname{atan}\left(\frac{\left(y^{start} + u_y^{start}\right) - \left(y^{end} + u_y^{end}\right)}{\left(x^{start} + u_x^{start}\right) - \left(x^{end} + u_x^{end}\right)}\right). \tag{13}$$

Using **Eqs 12**, **13**, the current length of the U-bolt $L + \Delta L$ can also be calculated, and the extension length ΔL can be acquired easily. It should be pointed out that ΔL is calculated in each iteration and updated all the time.

3.4 Tensile Strength Reinforcement of Bolt Elements

Once the extension length ΔL is acquired in each simulating iteration, the enhanced tensile strength is calculated using **Eq. 11**.

TABLE 6 | Mechanical properties of the simulated slope.

	Origin rock mass	Fractured rock mass	Failed rock mass (residual)
Density (kg/m^3)	2.5	2.5	2.5
Elastic modulus (GPa)	10	10	10
Poisson's ratio	0.3	0.3	0.3
Cohesion strength (MPa)	0.15	0.01	0.01
Friction angle (°)	20	20	40
Tensile strength (MPa)	5	1	1
Critical plastic strain (‰)	0	2	4

Then, it is added to the current tensile strength and cohesion of the bolt elements. This process occurs all the time for all the U-bolt elements, which indicates that the tensile strength and cohesion of the U-bolt element vary with the calculation.

4 APPLICATION IN ROCK ENGINEERING

4.1 Case 1: Rock Tunnel Excavation

4.1.1 Simulation Preparation

Figure 10 provides the simulation setup of the rock tunnel excavation. **Figure 10A** is the no supporting case, and **Figure 10B** is the case with U-bolt supporting. The size is set to be 60 m × 60 m. Vertical displacements on the top and bottom edges are fixed to zero, and horizontal displacements on the left and right edges are also fixed to zero. The element numbers of these two grids are about 3,000. The tunnel is set up in the middle of the grid, and the radius of the tunnel is 8 m. For the U-bolt-supporting cases (**Figure 10B**), a U-bolt is installed at the bottom left point after excavation, and the length of the U-bolt is about 8 m.

The crustal stress information is shown in **Table 3**, the rock mass properties are listed in **Table 4**, and the U-bolt parameters are provided in **Table 5**. The cohesion-weakening and friction-strengthening (CWFS) model is chosen as the constitutive model (Hajiabdolmajid et al., 2002; Feng et al., 2021). It should be noted that the U-bolt length and corresponding strength are set to be long and strong in order to make results more evident.

4.1.2 Performance of Umbrella-Shaped Bolts

The equivalent plastic strain (Hajiabdolmajid and Kaiser, 2003; Faleskog and Barsoum, 2013) can be applied to reflect the failure degree and the depth of excavation damaged zone. **Figure 11** shows the simulated equivalent plastic strain results of two cases. For the no support case (**Figure 11A**), the bottom left part seems to be symmetrical to the top right part, and the equivalent plastic strain for the most seriously damaged area is about 0.005.

For the U-bolt support case (**Figure 11B**), the equivalent plastic strain result is not symmetrical for the bottom left part and the top right part. Regarding the bottom left part, the shape of EDZ sank to the tunnel-free face and the depth of EDZ became smaller. Meanwhile, the equivalent plastic strain for the most seriously damaged area in the bottom left part is about 0.004.

Figure 12 compares the displacement evolution results along the bolt direction for no support and support with U-bolt cases. The tangential displacement along the bolt direction for the U-bolt supporting case is significantly inhibited. It changes from about 1 cm for the no support case to about 2 mm for the U-bolt-supporting cases, reducing about 80%. Moreover, the displacement along the bolt direction becomes gentler than that in the fluctuant circumstance of the no support case, indicating the U-bolt makes the rock mass deform globally and entirely.

4.2 Case 2: Rock Slope

4.2.1 Simulating Preparation

Figure 13 illustrates the simulation setup of the rock slope. As shown in **Figure 13A**, the size is set to be 100 m × 40 m, and vertical displacements on the bottom edges are fixed to zero, and horizontal displacements on the left and right edges are also constrained to zero. Meanwhile, **Figure 13B** is the no supporting case, and **Figure 10C** is the U-bolt supporting-case. For the U-bolt-supporting case (**Figure 10C**), the length of each U-bolt is 11.31 m, and they are installed at the slope body, which are perpendicular to the slope surface.

Three kinds of U-bolts are set, including 1# (3 m vertical distance from the slope feet), 2# (9 m vertical distance from the slope feet), and 3# (15 m vertical distance from the slope feet). In addition, four simulation cases are conducted: no support case, support case with 1# U-bolt, support case with 1# and 2# U-bolts, and support case with 1#, 2#, and 3# U-bolts. The rock mass properties are given in **Table 6**, and the U-bolt parameters are provided in **Table 5**. Furthermore, the CWFS model is used.

4.2.2 Performance of Umbrella-Shaped Bolts

The maximum principal stress contours for all four cases are shown in **Figure 14**. The tensile stresses on elements with U-bolts are definite for all supporting cases (**Figures 14B–D**) comparing the no support one (**Figure 14A**). It indicates that the U-bolt can provide a tensile anchorage force constraining the landslide distance. Another finding of the tensile anchorage stress is illustrated in **Figure 15**. With the increase in the U-bolt extension, the tensile stresses of element with U-bolt increase, which matches with the basic design of U-bolts in **Section 2.1** and operation description **Figure 2**.

The displacement contours of four simulation cases are shown in **Figure 16**. For the no support case in **Figure 16A**, the maximum displacement is larger than 0.07 m, and the sliding volume (here, it is considered as an area whose displacement is greater than 0.03 m in the dashed area in **Figure 16**) is large. For the support case with 1# U-bolt in **Figure 16B**, the maximum displacement is about 0.06 m. For the support case with 1# and 2#

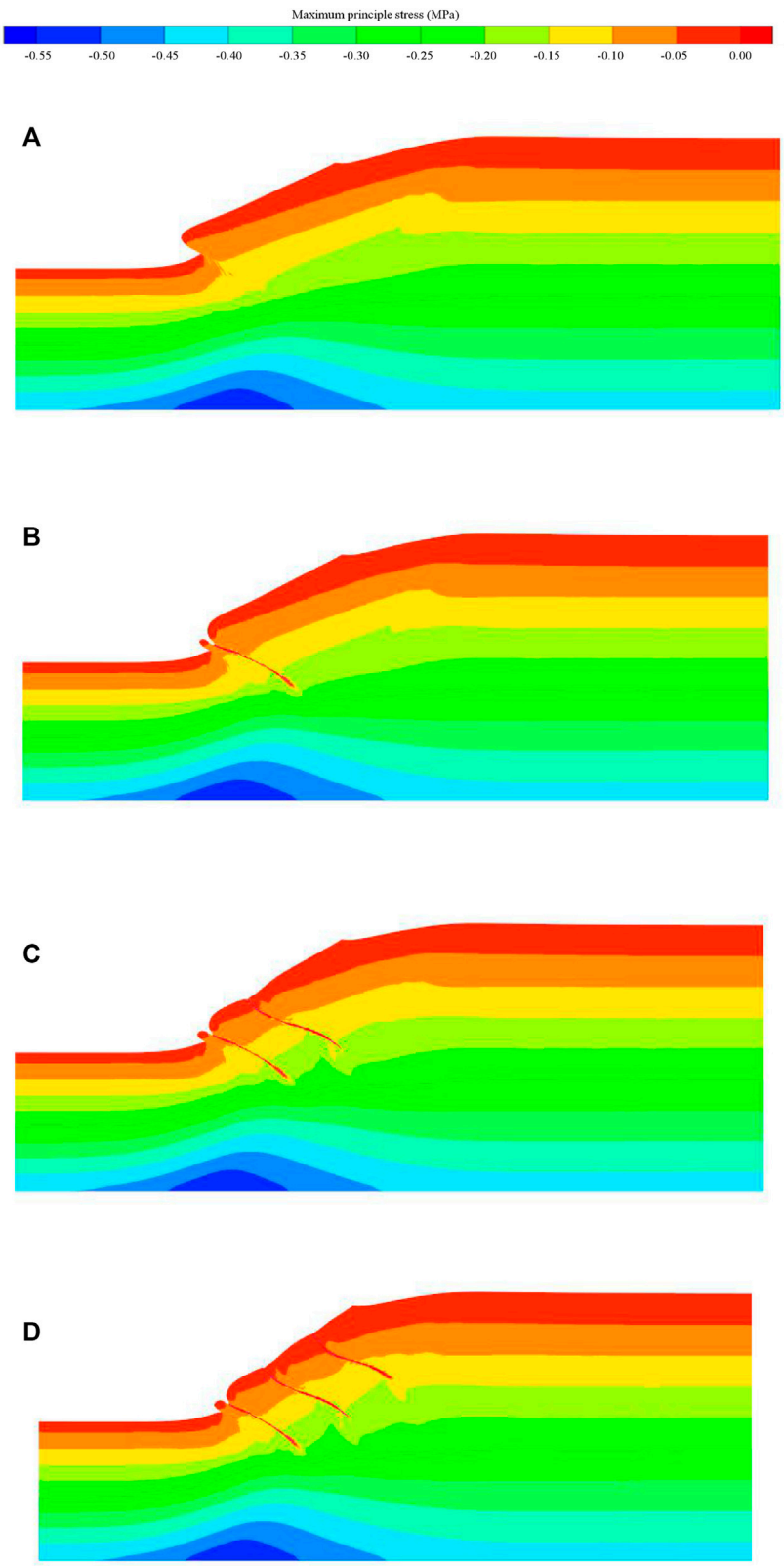

FIGURE 14 | Maximum principle stress contours, in which **(A)** no support, **(B)** support with 1# U-bolt, **(C)** support with 1# and 2# U-bolts, and **(D)** support with 1#, 2#, and 3# U-bolts.

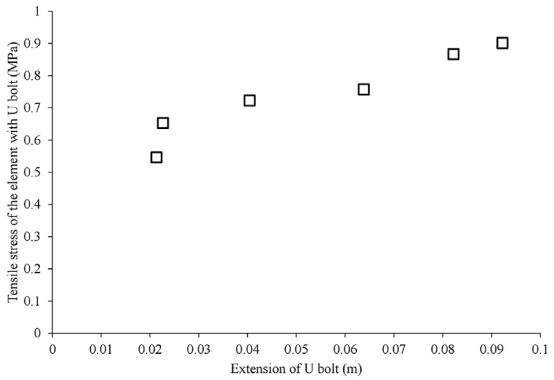

FIGURE 15 | Tensile stresses of elements with U-bolts plotted against the extension of U-bolts.

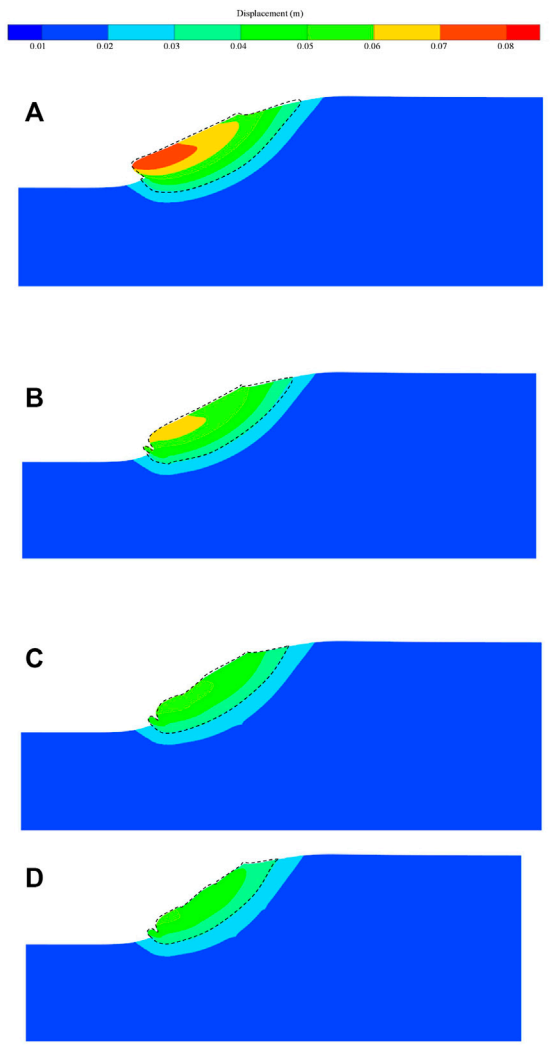

FIGURE 16 | Displacement contours, in which **(A)** no support, **(B)** support with 1# U-bolt, **(C)** support with 1# and 2# U-bolts, and **(D)** support with 1#, 2#, and 3# U-bolts.

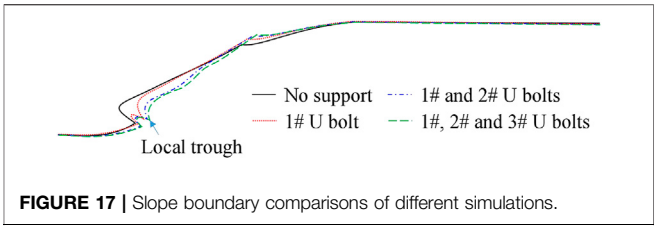

FIGURE 17 | Slope boundary comparisons of different simulations.

U-bolts (**Figure 16C**) and support case with 1#, 2#, and 3# U-bolts (**Figure 16D**), the maximum displacement is about 0.05 m. Results indicate that the U-bolts can decrease the maximum displacement and sliding volume efficiently.

Moreover, the slope boundary comparisons of different simulation cases are illustrated in **Figure 17**. It can be observed that the local constraining effect is evident, especially for 1# U-bolt near the slope feet, as local troughs emerge for the slope boundary. For the green dashed line (support case with 1#, 2#, and 3# U-bolts), the global constraining effect is prominent since the existence of 1#, 2#, and 3# U-bolts. Generally, due to the existence of the U-bolt, the decrease in the landslide distance is evident, and the global anchoring effect becomes better and better with the increase in the U-bolt number.

5 CONCLUSIONS AND DISCUSSIONS

A novel type of rock bolt, that is, the U-bolt was proposed in this study. The basic information was introduced at first, and the mechanical analysis was conducted to study the U-bolt reinforcement mechanism. In order to verify the real performance of the U-bolt, a numerical model has been established and then it was applied to the rock tunnel excavation simulation. Results reveal the rationality of the initial design goal of the U-bolt. Some important conclusions can be drawn as follows:

1) This friction and the tensile strength of the U-bolt will inhibit the dilation of the rock mass. The operating mechanism is that the tension of the bolt is converted into the extrusion force on the rock mass, which makes the U-bolt different from other rock bolts. Meanwhile, based on the characteristics of the U-bolt, the bolt can continuously compress the rock mass, and the higher compressive strength of the rock mass is used to obtain the greater friction force and anchoring force.
2) A mechanical model of U-bolt was proposed, and it concentrated on the enhanced tensile strength calculation method on the basis of structural analysis and the relation between penetration and point normal stress.
3) The proposed U-bolt mechanical model has been implemented through the identification of bolt elements, the calculation of the penetration, and the tensile strength reinforcement of bolt elements. The rock tunnel excavation simulations reveal that the U-bolt can reduce the tangential displacement along the bolt and EDZ depth, and alleviate the failure degree. Moreover, the U-bolt can also decrease the landslide distance by providing adequate anchorage force and stress with the extension.

DATA AVAILABILITY STATEMENT

The original contributions presented in the study are included in the article/supplementary material, further inquiries can be directed to the corresponding author.

AUTHOR CONTRIBUTIONS

YX: conceptualization and methodology; HC: data curation and writing—original draft preparation; YC: writing—review and editing, and project administration; SH: supervision; ZW: software and visualization; and YG: formal analysis.

FUNDING

The authors sincerely acknowledge the financial support from the National key R&D projects of China (grant No. 2017YFC1501303) and the Fundamental Research Funds for Central Public Welfare Research Institutes (grant No. CKSF2021460/YT).

ACKNOWLEDGMENTS

The authors express their gratitude to the State Key Laboratory of Geomechanics and Geotechnical Engineering, Institute of Rock and Soil Mechanics, Chinese Academy of Sciences.

REFERENCES

Aydan, Ö., and Kawamoto, T. (1992). The Stability of Slopes and Underground Openings against Flexural Toppling and Their Stabilisation. *Rock Mech. Rock Engng* 25 (3), 143–165. doi:10.1007/bf01019709

Bizjak, K. F., and Petkovšek, B. (2004). Displacement Analysis of Tunnel Support in Soft Rock Around a Shallow Highway Tunnel at Golovec. *Eng. Geology.* 75 (1), 89–106. doi:10.1016/j.enggeo.2004.05.003

Cai, Y., Esaki, T., and Jiang, Y. (2004). A Rock Bolt and Rock Mass Interaction Model. *Int. J. Rock Mech. Mining Sci.* 41 (7), 1055–1067. doi:10.1016/j.ijrmms.2004.04.005

Chen, Y. (2014). Experimental Study and Stress Analysis of Rock Bolt anchorage Performance. *J. Rock Mech. Geotechnical Eng.* 6 (5), 428–437. doi:10.1016/j.jrmge.2014.06.002

Faleskog, J., and Barsoum, I. (2013). Tension–torsion Fracture Experiments—Part I: Experiments and a Procedure to Evaluate the Equivalent Plastic Strain. *Int. J. Sol. Structures* 50 (25-26), 4241–4257. doi:10.1016/j.ijsolstr.2013.08.029

Feng, X. T., Wang, Z., Zhou, Y., Yang, C., Pan, P. Z., and Kong, R. (2021). Modelling Three-Dimensional Stress-dependent Failure of Hard Rocks. *Acta Geotechnica* 16 (6), 1647–1677. doi:10.1007/s11440-020-01110-8

Hajiabdolmajid, V., and Kaiser, P. (2003). Brittleness of Rock and Stability Assessment in Hard Rock Tunneling. *Tunnelling Underground Space Technol.* 18 (1), 35–48. doi:10.1016/s0886-7798(02)00100-1

Hajiabdolmajid, V., Kaiser, P. K., and Martin, C. D. (2002). Modelling Brittle Failure of Rock. *Int. J. Rock Mech. Mining Sci.* 39 (6), 731–741. doi:10.1016/s1365-1609(02)00051-5

Lee, J. R. (1997). The Law of Cosines in a Tetrahedron. *Pure Appl. Maths.* 4 (1), 1–6.

Li, C. C. (2010). A New Energy-Absorbing Bolt for Rock Support in High Stress Rock Masses. *Int. J. Rock Mech. Mining Sci.* 47 (3), 396–404. doi:10.1016/j.ijrmms.2010.01.005

Li, C. C. (2012). Performance of D-Bolts under Static Loading. *Rock Mech. Rock Eng.* 45 (2), 183–192. doi:10.1007/s00603-011-0198-6

Li, C. C., Stjern, G., and Myrvang, A. (2014). A Review on the Performance of Conventional and Energy-Absorbing Rockbolts. *J. Rock Mech. Geotechnical Eng.* 6 (4), 315–327. doi:10.1016/j.jrmge.2013.12.008

Liu, J., Wang, J., and Xu, T. (2018). Research of Swelling Prestressed Bolts Using inMechanized Excavation of Large Section Tunnel. *Tunnel Construction* 38 (z2), 324–329. doi:10.3973/j.issn.2096-4498.2018.S2.044

Renard, Y. (2006). A Uniqueness Criterion for the Signorini Problem with Coulomb Friction. *SIAM J. Math. Anal.* 38 (2), 452–467. doi:10.1137/050635936

Su, G., Feng, X., Wang, J., Jiang, J., and Hu, L. (2017). Experimental Study of Remotely Triggered Rockburst Induced by a Tunnel Axial Dynamic Disturbance under True-Triaxial Conditions. *Rock Mech. Rock Eng.* 50 (8), 2207–2226. doi:10.1007/s00603-017-1218-y

Varden, R., Lachenicht, R., Player, J., Thompson, A., and Villaescusa, E. (2008). "Development and Implementation of the Garford Dynamic Bolt at the Kanowna Belle Mine," in Proceedings of the 10th Underground operators Confenrence 19, Launceston, TAS, April 14–16, 2008 95–102.

Wang, B., and He, C. (2011). Application of Prestressed Hollow Grouting Anchor Rod in Rockburst Prevention Design of CangLing Tunnel. *Highway* (10), 206–210.

Wang, Z., Feng, X.-T., Yang, C., Zhou, Y., Xu, H., Han, Q., et al. (2020). Experimental Investigation on Fracturing Process of marble under Biaxial Compression. *J. Rock Mech. Geotechnical Eng.* 12 (5), 943–959. doi:10.1016/j.jrmge.2020.05.002

Zheng, Y., Chen, C., Liu, T., and Ren, Z. (2021). A New Method of Assessing the Stability of Anti-dip Bedding Rock Slopes Subjected to Earthquake. *Bull. Eng. Geol. Environ.* 80, 3693–3710. doi:10.1007/s10064-021-02188-4

Zheng, Y., Chen, C., Liu, T., Zhang, H., Xia, K., and Liu, F. (2018). Study on the Mechanisms of Flexural Toppling Failure in Anti-inclined Rock Slopes Using Numerical and Limit Equilibrium Models. *Eng. Geology.* 237, 116–128. doi:10.1016/j.enggeo.2018.02.006

Conflict of Interest: Author YG was employed by company PowerChina Huadong Engineering Corporation Limited.

The remaining authors declare that the research was conducted in the absence of any commercial or financial relationships that could be construed as a potential conflict of interest.

Publisher's Note: All claims expressed in this article are solely those of the authors and do not necessarily represent those of their affiliated organizations, or those of the publisher, the editors, and the reviewers. Any product that may be evaluated in this article, or claim that may be made by its manufacturer, is not guaranteed or endorsed by the publisher.